Journal of Physics D: Applied Physics, Volume 53, Number 7, 2020, Article number 075202
DOI: 10.1088/1361-6463/ab5758

Laser induced arc dynamics destabilization in laser-arc hybrid welding

Zhongyan Mu[1], Xin Chen[2], Renzhi Hu[1], Sanbao Lin[3], Shengyong Pang[1,*]

1. State Key Laboratory of Materials Processing and Die & Mould Technology,

Huazhong University of Science and Technology, China

2. Welding Engineering and Laser Processing Centre, Cranfield University, UK

3. State Key Laboratory of Advanced Welding and Joining, Harbin Institute of Technology, China

* Corresponding author: spang@hust.edu.cn

Abstract

The interaction between laser and arc plasma is a central issue in laser-arc hybrid welding. We report a new interaction phenomenon called laser destabilizing arc dynamics in kilowatt fiber laser-TIG hybrid welding of 316L stainless steel. We found the laser action significantly oscillates the arc tail with a 1~3 kHz high frequency. Direct numerical simulation demonstrates that the destabilization mechanism is due to the high-speed oscillated metal vapor ejecting from the mesoscopic keyhole. More interesting, the high-speed metal vapor could contrict the arc plasma by physical shielding. This provides a fundamentally different explanation from the generally adopted metal vapor ionization theory for laser constrict arc plasma phenomenon. Also, the results substantiate that the arc plasma cannot easily enter into the keyhole because of the violent metal vapor.

Keywords: hybrid welding; arc plasma; laser-induced vapor; keyhole.

1. Introduction

Since the invention of laser-arc hybrid welding (LAHW) in the 1980s, the interaction between laser and arc plasma has been a central issue in LAHW. In this process, the laser can promote arc igniting and burning [1-3]. The sysnergistic interaction of laser and arc (as known as the "1+1>2" effect) can significantly improve melting efficiency [4-6]. The laser can also improve weld quality [2,7,8]. Hence, it is generally recognized that the arc plasma can be stabilized by laser in the welding [9-11].

However, many studies demonstrated that in laser-TIG hybrid welding(LTHW), the arc is no longer in a steady state comparing to that in TIG welding. It implies that the laser also seems to

destabilize arc plasma in LAHW at the same time. For instance, in YAG LTHW, Natio et al. [12] observed a high-frequency arc plasma oscillation in the order of several kHz that is close to the oscillation frequency of keyhole in laser welding. Reisgen et al. [13] found that the electric signal of the arc becomes more unsteady and has more noises after either a CO_2 or a YAG laser was applied in the TIG welding process. Later, Natio et al. [14] observed that when the laser was applied in TIG welding, the arc voltage also exhibits violent oscillations, and the higher the laser power, the more severe the voltage oscillation. Schnick et al. [15] obtained similar conclusion in laser-TIG welding of ferrous alloys. These findings suggest that further studies are needed to elucidate the interesting role of laser on the stability of arc plasma in LAHW.

Here, the role of laser on the stability of arc plasma in fiber LTHW are systematically investigated by combining experiments and advanced numerical simulations. The high-speed video camera with an 808 nm band filter is used to observe the evolution of the arc shape. The unified laser-TIG model [16] used in this work considers the complex interaction between laser and arc. We experimentally and theoretically demonstrate that the laser action significantly constricts arc and oscillates the arc tail with a 1~3 kHz high frequency. The mechanisms of laser induced arc dynamics destabilization (LIADD) phenomenon is discussed in detail. For the first time, a physical picture that there are laser stabilization arc plasma and laser destabilization arc dynamics at the same time in a single laser hybrid welding is demonstrated and explained.

2. Materials and methods

2.1. Experiment procedure

The experimental platform of LTHW is set (**Fig. 1**). Experiments are performed by using a fiber laser welding machine (YLR-4000) and a TIG welding machine (Fronius TPS 400). The laser focus radius is 0.3mm. The defocus distance is 0 mm. The tungsten electrode diameter is 2mm with a cone tip of 60°, and the tip is located 5 mm above the workpiece surface. Bead-on-plate experiments are carried out. The plate is 316L stainless steel, and the thickness is 5 mm. To know the influences of varies parameters on arc behaviors clearly, the laser power, arc current, and the distance between the laser beam and arc cathode (DLA) are changed. The experimental parameters are shown in Table 1. TIG welding without laser action are conducted as controls. The flow rate of shielding gas (pure argon) is 15 L/min. Before welding, the plates are cleaned with acetone and are

scratched brush to avoid the influence of oxide film and grease.

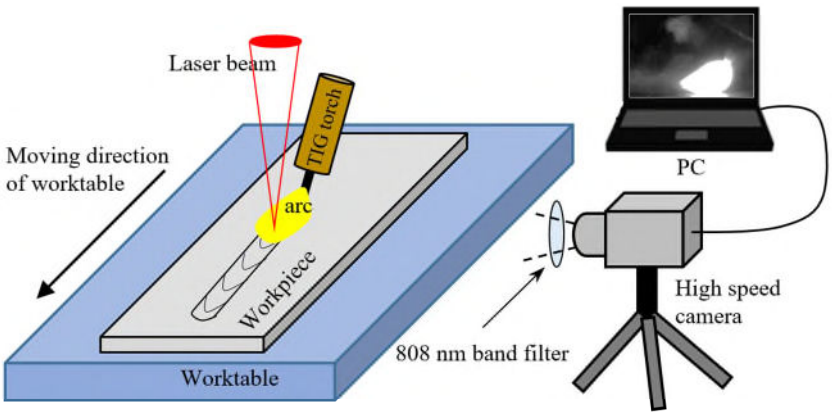

Figure 1. Digram of experimental setup.

To observe the arc behaviors, a high-speed video camera (phantom V-Series 611 high-speed camera) is used in experiments. The camera is placed the side, and the view direction is perpendicular to the welding path. An 808 nm narrow-band filter with 8 nm bandwidth is sited in front of the camera lens. Only some argon element spectrum can pass the filter (such as Ar I 810.369 and Ar I 811.531), while the metal vapor radiation light will be filtered out. The spectral intensity of the same element can roughly reflect the temperature, and the arc images obtained has a high temperature in the bright area. In addition, the distribution of metal vapor can be also observed by the reflection of argon arc light by fine particles of condensation. To capture the transient behavior of the arc, the frequency is as high as 5000 fps, and the exposure is 3 μs. The color mode of camera is grayscale, and the gain settings are same in all experiments.To facilitate the acquisition and processing of arc shape, the laser head, and arc torch are fixed, while the workpiece moved with the worktable.

To measure the area oscillation of the arc, binarization processing of the images is carried out. **Fig. 2**(a) shows the original arc grayscale image. The image is binarized with a certain threshold. For this study, the threshold is set at 230. Then arc area is obtained by counting pixels in the white region of the binarized image (Fig. 2(b)). The curve of the arc area evolution is obtained by measuring 500 images within 100 ms in quasi-steady state.

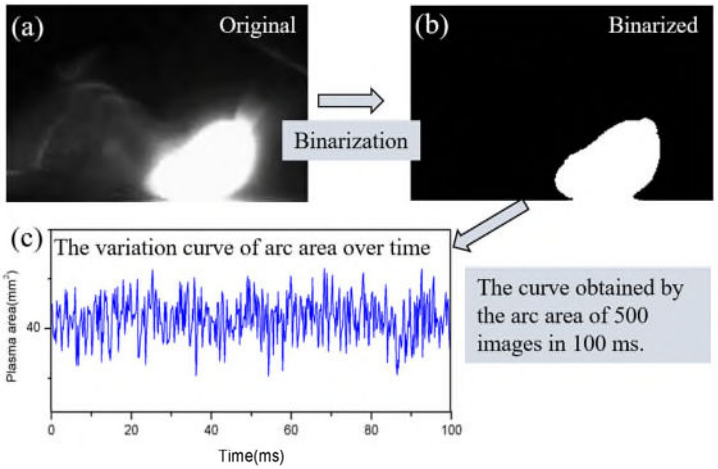

Figure 2. The binarization process of arc images.

Table 1
Experimental parameters

Process No.	Welding current (A)	Laser power (kW)	D_{LA} (mm)	Welding speed (m/min)
1	100	0	_	1.0
2	150	0	_	1.0
3	200	0	_	1.0
4	100	2.0	4	1.0
5	150	2.0	4	1.0
6	200	2.0	4	1.0
7	150	1.0	4	1.0
8	150	2.5	4	1.0
9	150	2.0	3	1.0
10	150	2.0	8	1.0

2.2. Modeling

Fig. 3 shows the diagram of LTHW process. To quantitatively study the laser-arc interactions, modeling was carried out with recently proposed laser-arc hybrid welding model in Ref [16]. Complex physical phenomena of LTHW are considered, including electrical, magnetic, flow, heat transfer, melting, evaporation, and so on. The model allows predicting the transient behaviors of LTHW, includes weld pool, arc plasma and vapor. For simple, some assumptions of arc plasma, vapor and weld pool have been made: (1) the arc plasma and the vapor are in LTE state, and the thermodynamic properties is a function of temperature and component. (2) the flows are laminar and incompressible Newtonian fluid. (3) the metal vapor is pure iron, the shielding gas is pure argon. (4) the arc plasma is optically thin.

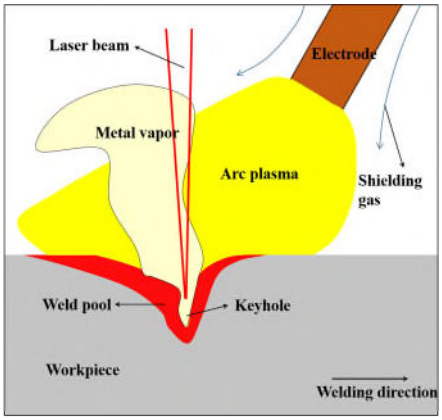

Figure 3. Diagram of LTHW process.

2.2.1. Modeling the laser-arc interaction

To accurately predict arc behaviors in LTHW, the laser-arc interaction needs to be considered. **Fig. 4** shows the interaction between the laser and arc. First, the laser can directly heat the arc as it passes through the arc [17, 18]. Second, the laser-induced metal vapor will change the composition, fluid flow and heat transfer of the arc plasma [9, 19]. Moreover, the arc and metal vapor will absorb the laser energy, which can change the laser energy efficiency.

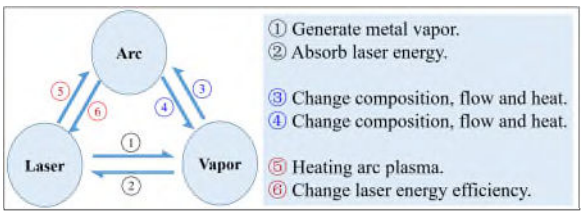

Figure 4. The interaction between laser and arc.

The laser energy can be absorbed by the arc and vapor, and hence producing a heating effect. For short-wavelength laser (such as fiber laser and YAG laser), the inverse bremsstrahlung absorption is very weak and negligible [18, 20]. However, the ultrafine particles in plume can absorb the laser energy due to Rayleigh scattering effect [21, 22]. The absorption rate $\eta = 5$ m^{-1} of ultrafine particles is used in this study [22, 23]. The absorption heating Q_{laser} from the laser energy is a volume source item for hybrid plasma (vapor, arc plasma, and shielding gas), which can be expressed by $Q_{laser} = (I_R A / \Delta V) \cdot (\eta \delta C_{vapor})$. I_R is the laser energy density. C_{vapor} is the metal vapor mass fraction. A and ΔV are the area and the volume of control element, respectively. δ is the length of the laser travels through control element.

A large amount of metal vapor ejects from the keyhole by laser action, which directly affects the flow and heat transfer behaviors of the arc. Moreover, the composition of the arc will be changed, and the physical parameters will also change accordingly. In the welding, the laser causes local evaporation of the weld pool, and then the surface of the weld pool can be divided into the evaporation region and non-evaporation region. In the evaporation region, the evaporation pressure as a flow boundary condition, and the vapor is pure iron $C_{vapor} = 1.0$. In the non-evaporation region,

the no-slip wall boundary condition is applied, and the boundary of vapor mass fraction is $\partial C_{vapor}/\partial \vec{n}=0$. These vapor will enter the arc plasma and mix. The distribution of vapor can be obtained by the vapor mass conservation equation [18]:

$$\frac{\partial}{\partial t}(\rho_g C_{vapor}) + \nabla \cdot (\rho_g \vec{u}_g C_{vapor}) = \nabla \cdot (\rho_g D \nabla C_{vapor}) \tag{1}$$

here, $\vec{u}_g$, ρ_g is the velocity and density of hybrid plasma, respectively. D is the diffusion coefficient, which can be obtained by second viscosity approximation from Ref [24]. Note that the diffusion coefficient D in Eq. 1 can be also obtained by combined diffusion coefficient method [25, 26].

The metal vapor could change the properties, thereby affecting the behaviors of the arc plasma. In the model, the thermophysical parameters of Fe-Ar mixture gas are considerd [16]. The parameters include density, thermal conductivity, specific heat, electrical conductivity, viscosity, and net emission coefficient. The thermophysical parameters of arc plasma is calculated according to the temperature and vapor mass fraction.

2.2.1. Governing equations

In this model, the electromagnetic field is modeled in the whole region. The heat and mass transfer behaviors are modeled separately in the mixture-fluid phase (solid and liquid) region and the hybrid plasma region. In this study, only important control equations are introduced. For more details, please refer to our previous work [16].

The charge continuity equation and Ohm's law are used to calculate the potential and current density in whole region. The mass, momentum, and energy equations are applied to calculate the heat and mass transfer behaviors. The Level-Set method is used to trace the interface of the weld pool. The laser heating for weld pool is calculated by ray tracing method.

(1) In the whole calculation region, electromagnetic equations are [16]:

$$\nabla \cdot \vec{j}=0 \tag{2}$$

$$\vec{j}=-\sigma_e \nabla \varphi \tag{3}$$

$$\nabla^2 \vec{A}=\mu_0 \vec{j}, \tag{4}$$

$$\vec{B}=\nabla \times \vec{A}, \tag{5}$$

where φ, $\vec{j}$, $\vec{A}$, $\vec{B}$ is the potential, current density, magnetic potential and magnetic field, respectively. σ_e, μ_0 is the electrical conductivity and vacuum permeability.

(2) In the hybrid plasma region, the mass, momentum and energy equations of hybrid plasma are [16]:

$$\frac{\partial \rho_g}{\partial t} + \nabla \cdot \left(\rho_g \vec{u}_g \right) = 0 ., \tag{6}$$

$$\frac{\partial}{\partial t}(\rho_g \vec{u}_g) + \nabla \cdot (\rho_g \vec{u}_g \vec{u}_g) = -\nabla P_g + \nabla \cdot \left(\mu_g (\nabla \vec{u}_g + \nabla \vec{u}_g^T - \frac{2}{3} \nabla \cdot \vec{u}_g) \right) + F_g , \tag{7}$$

$$\frac{\partial (\rho_g h_g)}{\partial t} + \nabla \cdot (\rho_g h_g \vec{u}_g) = \nabla \cdot (k_g \nabla T_g) - 4\pi \varepsilon_N + S_e + Q_{laser} , \tag{8}$$

where $\vec{u}_g$, P_g, T_g, and h_g is the velocity, pressure, temperature and enthalpy. ρ_g, μ_g, C_{pg}, k_g and ε_N is density, viscosity, specific heat, thermal conductivity and net emission coefficient. F_g is the external force that includes gravity and Lorentz force. S_e includes Joule heating and electron thermal transport.

Note that the subscript ‘g’ and ‘m’ indicate the hybrid plasma region and the mixture fluid phase region, respectively.

(3) In the mixture-fluid phase region, the mass, momentum and energy equations are [27]:

$$\nabla \cdot \vec{u}_m = 0 \tag{9}$$

$$\frac{\partial}{\partial t}(\rho_m \vec{u}_m) + \nabla \cdot (\rho_m \vec{u}_m \vec{u}_m) = \nabla \cdot (\mu_m \nabla \vec{u}_m) - \nabla P_m + F_m \tag{10}$$

$$\rho_m C_{pm} \left(\frac{\partial T_m}{\partial t} + (\vec{u}_m \cdot \nabla) T_m \right) = \nabla \cdot (k_m \nabla T_m) , \tag{11}$$

where F_m is the external volume force of the weld pool suffered, includes Lorentz force, buoyancy force and Dacy force. The mixture modle is used to treat the solid-liquid interface [28]. The Joule heating is omitted in the weld pool.

(4) For tracing the interface,the Level-Set method is used to trace the interface of weld pool, and the equation is [29]:

$$\frac{\partial \phi}{\partial t} + \vec{u}_m \cdot (\nabla \phi) = 0 , \tag{12}$$

where ϕ represents a signed distance function , and the interface of weld pool is determined by ϕ=0 .

2.2.3. Boundary conditions

In the developed model, the energy, momentum and electromagnetic boundary conditions are treated.

(1) Energy boundary conditions

At the interface of two calculation regions, thermal conduction, electron condensation, radiation, evaporation are considered for mixture-fluid phase, while only thermal conduction is considered for hybrid plasma.

$$q_{metal} = q_{laser} + q_{cond} + q_e - q_{rad} - q_{evp} \tag{13}$$

$$q_{gas} = -q_{cond} \tag{14}$$

$$q_{cond} = k_{eff}(T_{gs} - T_{ms}) / \delta_{eff} \tag{15}$$

$$q_{elec} = \left|\vec{j} \cdot \vec{n}\right| \varphi_a \tag{16}$$

$$q_{rad} = \varepsilon_r k_B (T_{ms}^4 - T_\infty^4) \tag{17}$$

$$q_{evp} = W_e L_v \tag{18}$$

(2) Momentum boundary conditions

For the mixture-fluid phase, the pressure and the shear stress boundary conditions can be expressed as:

$$P_f = \gamma\kappa + P_{eff} + 2\mu_m \vec{n} \cdot \nabla\vec{u}_m \cdot \vec{n} \tag{19}$$

$$\vec{\tau} = -\mu_g \frac{\partial(\vec{u}_g \cdot \vec{s})}{\partial\vec{n}} + \frac{\partial\gamma}{\partial T_m}\frac{\partial T_m}{\partial\vec{s}} \tag{20}$$

where $P_{eff} = \max(P_r, P_g)$, and P_r is recoil pressure.

For the hybrid plasma, the non-evaporation zone on the weld pool surface is treated as a wall boundary. At the evaporation zone, the plasma is mainly driven by the recoil pressure

$$P_{gb} = P_r \tag{21}$$

On the weld pool surface, the metal vapor mass fraction is considered as $C_{vapor} = 1.0$ at the evaporation zone, and $\partial C_{vapor} / \partial\vec{n} = 0$ at the non-evaporation zone.

(3) Electromagnetic boundary conditions

The electric potential is set to be zero on the bottom surface of anode. The electric potential boundary condition of cathode tip surface is

$$\begin{cases} -\sigma_e \dfrac{\partial \varphi}{\partial \vec{n}} = j_c, & r \le R_c \\ -\sigma_e \dfrac{\partial \varphi}{\partial \vec{n}} = 0, & r > R_c \end{cases} \tag{22}$$

where the current density j_c is set as $6.5\times10^7\, A/m^2$. R_c is the cathode spor radius and calculated as $R_c=\sqrt{I/(\pi j_c)}$. I is the welding current.

2.2.4. Implement

The unified model was discrete by FDM and implemented by C++ programming. The welding process during LTHW of 316L stainless steel was simulated using the unified model. The simulations used the same physical parameters as the experiment. To avoid computation too expensively, a small calculation region (14 mm × 10 mm × 13 mm) was used. The uniform mesh sizes with 0.1 mm were used in this study.

3. Results and discussion

3.1. Laser destabilizing arc dynamics phenomenon

Fig. 5 and **Fig. 6** show the high-speed images of TIG and LTHW arc, respectively. It can be found that the TIG arc is quite stable and large with an elongated arc tail, while the LTHW arc is small and oscillated. As shown in **Fig. 5**, the arc doesn't change obviously over time. The arc area increases as the current increases due to the more Joule heat. **Fig. 6** shows that the LTHW arc is significantly smaller than the TIG arc, and the arc area changes dramatically over time. When the current is 100A, the LTHW arc area at 0.8 s is only half of that at 0.6 s. The arc area change occurs mainly at the arc tail and remains stable near the cathode. Further, lots of metal plume can be found behind arc tail. The laser-induced arc area decrease and arc oscillation occur under different welding current. From above, it is inferred that the laser can destabilize arc dynamics in LTHW.

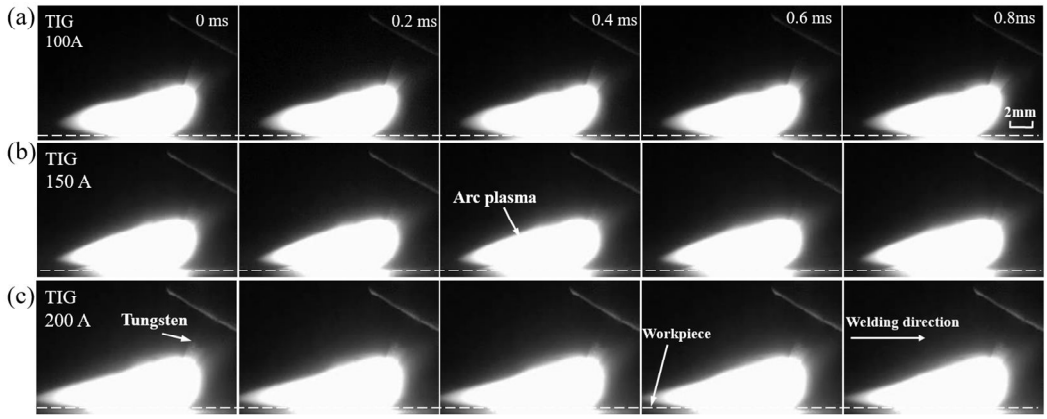

Figure 5. The high-speed images of stable TIG arc under different welding current.

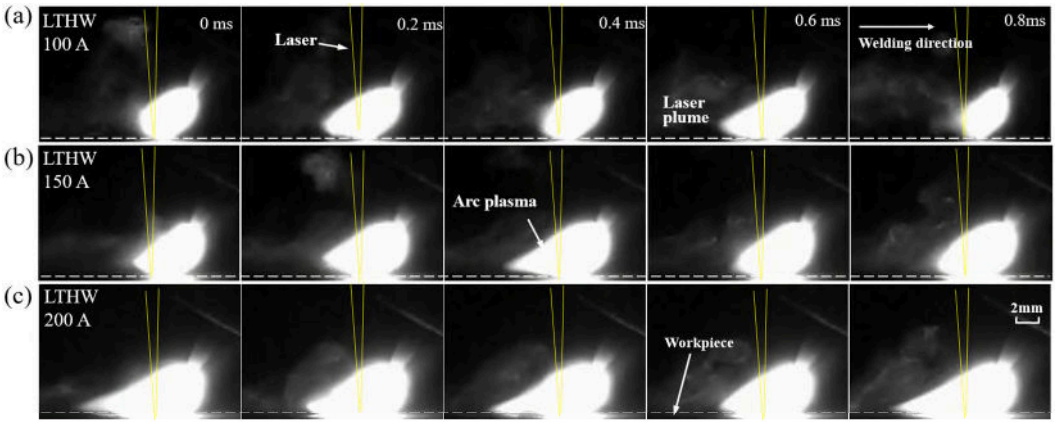

Figure 6. The high-speed images of oscillated LTHW arc under different welding current.

For studying the oscillation behaviors of the arc, **Fig. 7** is provided to show the evolutions of TIG arc and LTHW arc areas under different currents. When the current is 100A, the TIG arc is quite stable, where the area fluctuation with a small amplitude (5.6 mm^2) and a low frequency (100-200 Hz). The LTHW arc is in a state of violent oscillation, the amplitude is 25.2 mm^2 and the frequency is increased to 1-3 kHz. This is consistent with Naito's results [12]. As the current increases, the LTHW arc oscillates at the same frequency. The constriction effect of laser on arc is weakened and the relative oscillated amplitude is reduced, that is, the LIADD phenomenon is weakened.

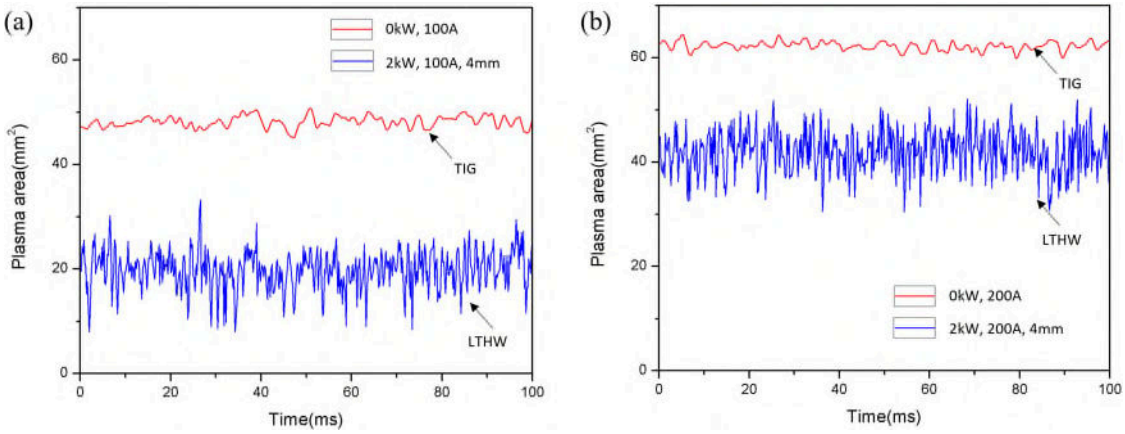

Figure 7. The curve of the TIG and LTHW arc area evolution: (a) 100 A; (b) 200 A.

Further, the influences of varies parameters have been studied, including laser power and D_{LA}. As shown in **Fig. 8**, the oscillation frequency of LTHW arc is the same, all of them are 1-3 kHz. However, the constriction and oscillation amplitude of the arc is different. As the increase of laser power or as the decrease of D_{LA}, the constriction degree and oscillation amplitude of the arc is increased. In addition, the influence of laser power on the arc area is less than that of D_{LA}.

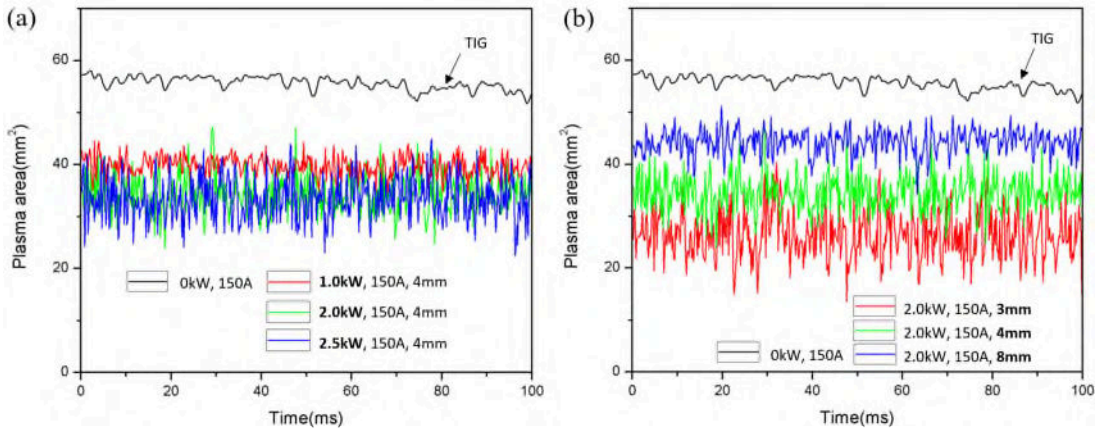

Figure 8. The curve of arc area evolution under different process parameters: (a) Different laser power; (b) Different D_{LA}.

In summary, the LIADD phenomenon can be found under different process conditions, which could be a general phenomenon in LTHW. This phenomenon is manifested by the fact that the laser-induced arc area decrease and arc oscillation. Under the laser action, the arc changes from a slightly low frequency (100-200 Hz) oscillation in TIG welding to a violent high frequency (1-3 kHz) oscillation in LTHW. In addition, lower welding currents, stronger laser power, and greater D_{LA} can lead to a more pronounced phenomenon of laser destabilizing arc dynamics.

3.2. Prediction of laser induced arc dynamics destabilization

Based on our recently proposed new model [16], we quantitatively analyzed the LIADD

phenomenon in LTHW of 316L stainless steel. **Fig. 9** shows the predicted temperature field of TIG and LTHW arc with a current of 100 A. The stable TIG arc has a high-temperature tail, while the LTHW arc is more complex in **Fig. 9**(b). First, the laser leads to a significant decrease in the temperature of the arc tail. Secondly, the temperature distribution of the LTHW arc is no longer stable over time as the TIG arc, but it is a periodic phenomenon of contraction and spread. As shown in **Fig. 9**(b), the arc has an elongated high-temperature tail (>10000 K) initially. Then, the elongated arc tail becomes shorter and even disappears gradually. As welding proceeds, the elongated high-temperature arc tail appears again. Then, the arc enters the oscillation of the next cycle, and the above evolution process is repeated. The duration of the above process is about 0.43 ms, which indicates that the simulated oscillation frequency is consistent experiments (1-3 kHz). The same phenomenon has been found in both simulation and experiment: the arc is constricted and in a state of oscillation under laser action.

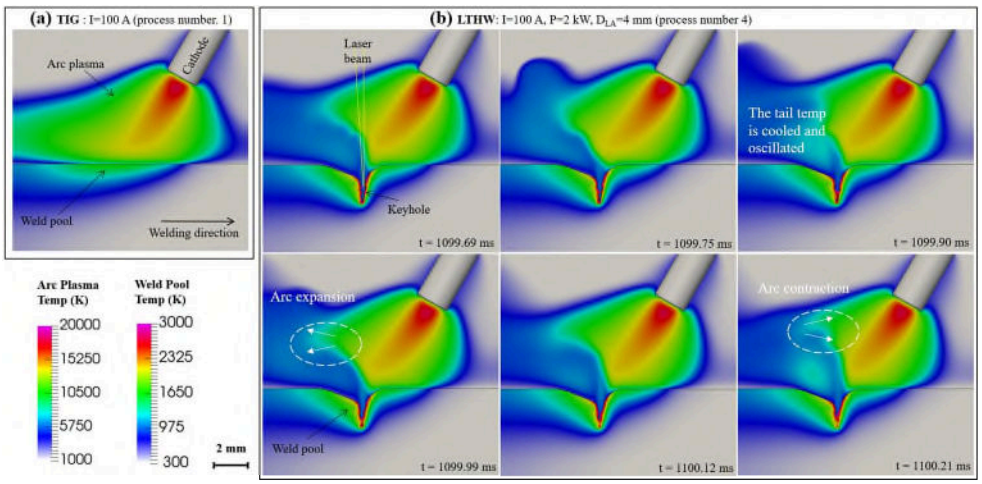

Figure 9. The predicted temperature field of TIG and LTHW arc with welding current 100 A: (a) TIG; (b) LTHW.

Further, the LTHW arc behaviors are simulated under different process parameters, including varying welding current, laser power, and D_{LA}. For the sake of simplicity, we only show the typical arc characteristics under different process conditions. As shown in **Fig. 10**, the high-temperature region of the arc decreases as the current decreases, the laser power increases or the D_{LA} decreases. That is consistent with the experimental results as shown in Section 3.1.

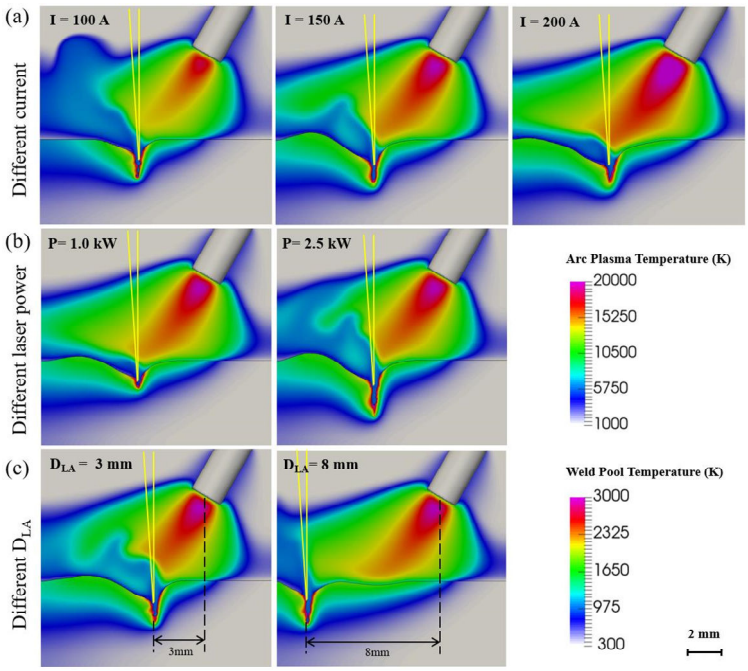

Figure 10. The predicted temperature field of LTHW arc under different process parameters: (a) Different welding current; (b) Different laser power; (c) Different D_{LA}.

3.3. The mechanism of laser induced arc dynamics destabilization

In LAHW, the impact of laser on arc includes the direct effect by heating and the indirect effect due to laser-induced metal vapor. For fiber laser, the direct heating effect primarily considers Rayleigh absorption effect due to ultrafine particles inside vapor plume. According to our previous work [30], this heating effect is nor dominant in fiber LTHW. Therefore, we mainly discuss the influence of laser-induced metal vapor.

Fig. 11 shows the distribution of metal vapor in hybrid plasma. The metal vapor is mainly distributed in the arc tail, while there is almost no vapor near the cathode. That is consistent with the spectral measurements in our previous work [30]. The metal vapor could have an impact on the electromagnetic and thermal dynamics of the arc. The impact of these two aspects will be discussed separately below.

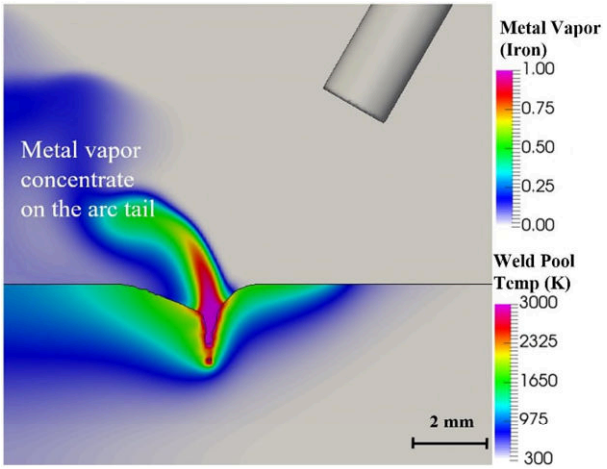

Figure 11. Predicted metal vapor distribution in LTHW(process number 4).

(1) The electromagnetic impact of metal vapor

Some researchers argue that laser-induced metal vapor can form conductive channel and leads a significant effect on arc plasma, such as contraction and attraction [10, 11]. To analyze the electromagnetic impact of metal vapor, the current density distribution of single TIG and LTHW are compared in **Fig. 12**. Compared TIG welding, the current density is smaller on arc tail and is greater slightly to the right of keyhole in LTHW. However, the difference in current density distribution between the TIG and LTHW arcs is still small. That is the metal vapor has only little effect on the current distribution of the arc in this study.

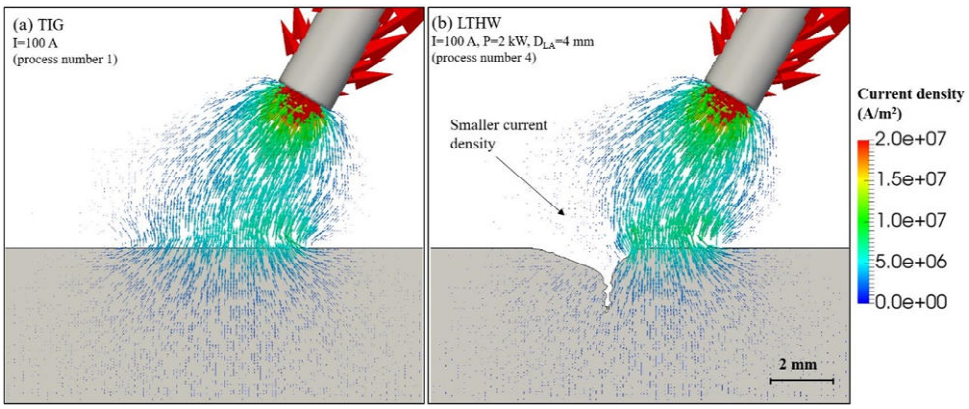

Figure 12. Predicted current density: (a) TIG (process number 1); (b) LTHW (process number 4).

Fig. 13(a) shows the electrical conductivity distribution of hybrid plasma, which is obtained based on the temperature and the vapor mass fraction distribution. The electrical conductivity in keyhole and arc tail is quite small where there the metal vapor is enriched. Kozakov et al. [31] found similar phenomena in GMAW experiments. They demonstrated a cold metal core pushing the

current conduction to an outer Ar shell. Here, it should be noted that the electrical conduction of the plasma is determined by both ionization potential and the temperature. Metal vapor is enriched inside the keyhole and at arc tail, the low temperature suppresses the ionization of the composite plasma. As shown in **Fig. 13**(b), when the temperature is 6000 K, the conductivity of pure iron vapor is only 20% of the argon plasma at 13000 K. That is to say that the laser-induced metal vapor is at low ionization degree. This is consistent with some other independent researches [32, 33], and this can also explain the phenomenon of arc voltage rise after laser action discovered by some researchers [14, 32].Summarily, the laser-induced metal vapor does not cause a large change in the current distribution under the conditions of this study. Therefore, the electromagnetic impact of laser and laser-induced metal vapor is hard to cause the LIADD phenomenon.

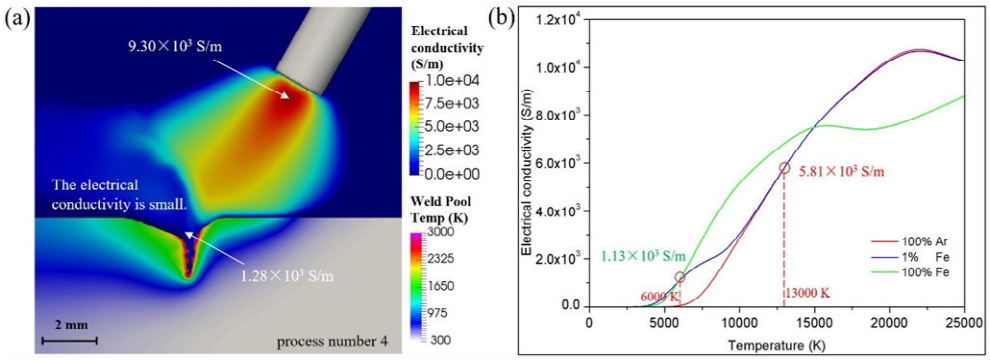

Figure 13. The electrical conductivity of hybrid plasma: (a) The electrical conductivity distribution of hybrid plasma, (b) The electrical conduction of iron-argon mixture gas[10].

(2) The thermal dynamics impact of metal vapor

Fig. 14 shows the predicted flow field and density distribution of hybrid plasma in LTHW. To study the dynamics of laser on the arc, we divide the flow of the hybrid plasma into arc flow and vapor flow. As shown in **Fig. 14**, the vapor flow has a significantly higher velocity and density than the arc flow. That is to say, the vapor flow has greater momentum. Therefore, a strong dynamics interaction will occur between the vapor flow and the arc flow. On the one hand, the vapor flow could physically shield arc flow at the arc tail, so that the arc flow velocity near the keyhole is slowed and the direction changes. On the other hand, under the side blow of the arc flow, the vapor flow is difficult to flow toward the electrode and eventually flows backward and upward. It easily concludes that the arc flow is also hardly entering the keyhole due to the violent vapor impacting.

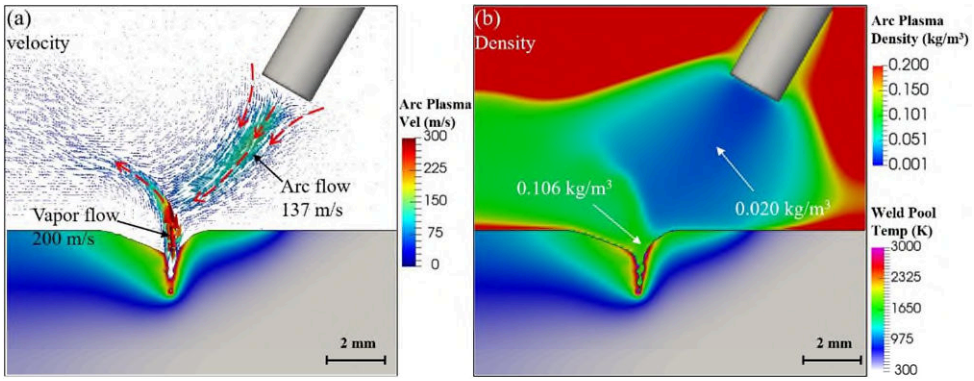

Figure 14. Predicted flow field and density distribution of hybrid plasma in LTHW.

The unique flow pattern is formed by the dynamic interaction of the vapor flow and the arc flow in **Fig. 14** (a), which obviously affects the arc temperature and metal vapor distribution through intense convection. The side blow of the arc flow on the vapor flow causes the metal vapor concentrating on the arc tail. Under the physical shielding effect of vapor flow, the heat transportation from high-temperature region to arc tail is limited. In addition, the cold metal vapor can cool the arc tail by convection cooling and radiation enhancement [30]. As a result, the temperature of the arc tail is decreased, the arc tail becomes shorter and the arc area decreased.

In hybrid welding, the vapor flow is not in a steady state but is always in a state of high-frequency oscillation. As shown in **Fig. 15**, the oscillated vapor flow causes different disturbances to the arc flow. When the injection velocity of vapor flow is decreased (**Fig. 15**(c)), the arc flow can produce a more pronounced side blow effect, and the impact of vapor flow on the arc flow is weakened. At this time, the arc expands and has a longer arc tail. When the injection velocity of vapor flow is increased (**Fig. 15**(d)), the vapor flow will overcome the side blow action of the arc flow, and the impact of vapor flow on the arc flow is enhanced. At this time, the arc constricts and has a shorter arc tail. As a result, the arc exhibits a periodic contraction and relaxation phenomenon under the action of high-frequency oscillated vapor flow, that is LIADD phenomenon. In addition, the arc oscillated frequency is similar to that of laser-induced metal vapor, which is about 1-3 kHz [34, 35].

The interaction between the vapor flow and the arc flow can also explain the difference of LIADD phenomenon under different process parameters. Increasing the laser power, the vapor flow can be enhanced. Reducing the welding current, the arc flow will be weakened. Shorten the D_{LA}, the interaction of vapor flow and arc flow can be enhanced. These can result in a more pronounced

LIADD phenomenon, as shown in **Fig. 7** and **Fig. 8**. Since the oscillation frequency of the metal vapor is always 1-3 kHz, the oscillation frequency of the arc is similar under different process conditions.

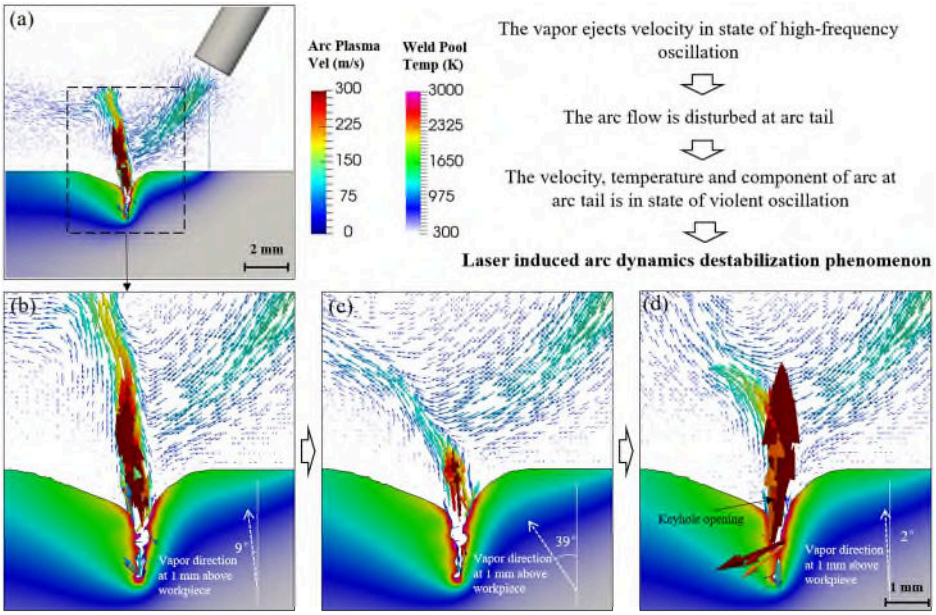

Figure 15. The dynamic evolution of arc and vapor flow near the keyhole (process number 4): (a) 1099.72 ms; (b) 1099.72 ms; (c) 1099.75 ms; (d) 1099.90 ms.

In summary, the mechanism of LIADD phenomenon in LTHW is the dynamic interaction of the high-speed and high-frequency oscillating metal vapor flow with the arc flow, nor the electromagnetic interaction. Resulting in arc flow, temperature and component disturbance. The arc area decreases obviously, and the arc oscillates with frequencies up to 1-3 kHz as same as laser-induced metal vapor. In addition, the arc is hardly enter into the keyhole due to the high-speed vapor and the low conductivity in the keyhole.

It needs to be stated that the LIADD phenomenon is not in conflict with the laser stable arc high-speed welding process, we still get a more stable welding quality as shown in **Fig. 16**. Actually, the LIADD phenomenon could have an important impact on the stability of arc high-speed welding. First, the high-frequency oscillation of arc due to the laser-induced vapor may improve the anti-interference ability of the arc. Then, the LIADD phenomenon could enhanced the turbulent diffusion of metal vapor, and these metal vapor could facilitate arc striking, avoid arc breaking and stabilize arc burning. This phenomenon can enriches the perspective of understanding the laser arc interaction in LAHW.

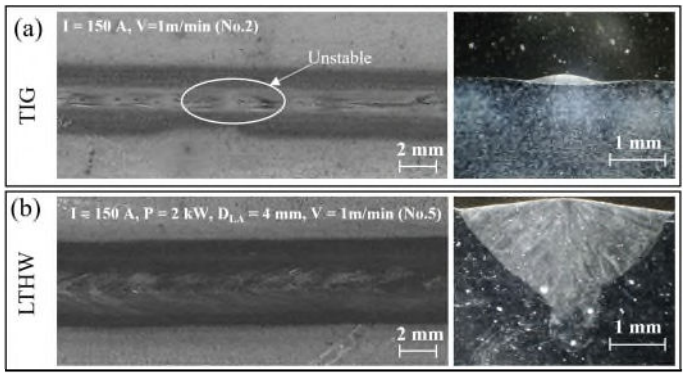

Figure 16. Comparison of weld seam between TIG and LTHW: (a) TIG; (b) LTHW.

The present work is focused on the process of kilowatt fiber laser arc hybrid welding of ferrous alloys. It is mentioned that different phenomena may occur in hybrid welding with lower power laser or for Al/Mg alloys [6, 15, 18]. The lower-power laser can only induced low vaporization rates and lead to small thermal dynamic impact. In the hybrid welding of Al/Mg alloys, the laser can remove the oxide layers. These phenomena and corresponding comprehensive explanations can be found in Ref [15].

4. Conclusion

The arc behaviors of kilowatt fiber laser-TIG hybrid welding (LTHW) of 316L stainless steel have been investigated by combining experiments and numerical simulations. The main conclusions are as follows:

1. Laser induced arc dynamics destabilization (LIADD) phenomenon has been found both in experiments and simulations, and the LIADD phenomenon usually appears in the arc tail region. Although the laser can improve the high-speed stability of the arc, it will make the arc oscillation more intense and make the arc area shrink. Under the laser action, the arc changes from a slightly low frequency (100-200 Hz) oscillation in TIG welding to a violent high frequency (1-3 kHz) oscillation in LTHW.

2. The oscillation of the LTHW arc has the same oscillation frequency (1-3 kHz) under different process parameters, while the arc shrinkage and oscillation amplitude are different. Lower welding currents, stronger laser power, and greater D_{LA} can lead to more pronounced LIADD phenomenon.

3. The mechanism of the LIADD phenomenon in LTHW is the dynamic interaction of metal vapor flow and the arc flow. In LTHW, the arc exhibits a periodic contraction and expansion phenomenon with a frequency of 1-3 kHz under the action of high-speed and high-frequency laser-

induced metal vapor.

4. In fiber LTHW, the arc plasma cannot easily enter into the keyhole because of the violent metal vapor. On the one hand, the vapor flow ejects from the keyhole with a high speed, and it is difficult for the arc flow to enter the keyhole. On the other hand, the metal vapor in the keyhole has low electric conduction due to low temperature (about 6000K), which leads the arc current is also difficult to enter the keyhole.

Acknowledgments

The authors are grateful to the support of the National Key R&D Program of China (No. 2017YFE0100100), the National Natural Science Foundation of China (No. 51675202) and State Key Laboratory of Advanced Welding and Joining.

Reference:

[1] Zhiyong L, Srivatsan TS, Yan LI, Wenzhao Z. Coupling of laser with plasma arc to facilitate hybrid welding of metallic materials: a review. *J Mater Eng Perform* 2013;22:384–95.

[2] Hu B, Den Ouden G. Laser induced stabilisation of the welding arc. *Sci Technol Weld Join* 2005;10:76–81.

[3] Kah P. Overview of the exploration status of laser-arc hybrid welding processes. *Rev Adv Mater Sci* 2012;30:112–32.

[4] Liu L, Hao X, Song G. A new laser-arc hybrid welding technique based on energy conservation. *Mate Trans* 2006, 47(6): 1611-1614.

[5] Hu B, Den Ouden G. Synergetic effects of hybrid laser/arc welding. *Sci Technol Weld Joi* 2005, 10(4): 427-431.

[6] Mahrle A, Schnick M, Rose S, Demuth C, Beyer E, Füssel U. Process characteristics of fibre-laser-assisted plasma arc welding. *J Phys D Appl Phys* 2011, 44(34): 345502.

[7] Meng Y, Gao M, Zeng X. Quantitative analysis of synergic effects during laser-arc hybrid welding of AZ31 magnesium alloy[J]. *Opt Lasers Eng* 2018, 111: 183-192.

[8] Wang L, Li X, Gao M, Zeng X. Stabilization mechanism and weld morphological features of fiber laser-arc hybrid welding of pure copper. *J Manuf Process* 2017, 27: 207-213.

[9] Ono M, Shinbo Y, Yoshitake A, Ohmura M. Development of laser-arc hybrid welding. *NKK Tech REPORT-JAPANESE Ed* 2002:70–4.

[10] Liu L, Chen M, Li C. Effect of electric arc on laser keyhole behavior based on direct observation during low power pulsed laser–arc hybrid welding process. *Opt Lasers Eng* 2013;51:1153–60.

[11] Meng Y, Gao M, Zeng X. Effects of arc types on the laser-arc synergic effects of hybrid welding. *Opt Express* 2018;26:14775–85.

[12] Naito Y, Mizutani M, Katayama S. Penetration characteristics in YAG laser and TIG arc

hybrid welding, and arc and plasma/plume behaviour during welding. Welding phenomena in hybrid welding using YAG laser and TIG arc (First Report). *Weld Int* 2006;20:777–84.

[13] Reisgen U, Krivtsun I, Gerhards B, Zabirov A. Experimental research of hybrid welding processes in combination of gas tungsten arc with CO2-or Yb: YAG-laser beam. *J Laser Appl* 2016;28:22402.

[14] Naito Y, Mizutani M, Katayama S. Electrical Measurement of Arc during Hybrid Welding-Welding Phenomena in Hybrid Welding Using YAG Laser and TIG Arc(Third Report)-. *Q J Japan Weld Soc* 2006;24:45–51.

[15] Schnick M, Rose S, Füssel U, Mahrle A, Demuth C, Beyer E. Experimental and numerical investigations of the interaction between a plasma arc and a laser. *Weld World* 2012, 56(3-4): 93-100.

[16] Chen X, Mu Z, Hu R, Liang L, Murphy AB, Pang S. A unified model for coupling mesoscopic dynamics of keyhole, metal vapor, arc plasma, and weld pool in laser-arc hybrid welding. *J Manuf Process* 2019;41:119–34.

[17] Cho YT, Na SJ. Numerical analysis of plasma in CO 2 laser and arc hybrid welding. *Int J Precis Eng Manuf* 2015;16:787–95.

[18] Mahrle A, Beyer E. Hybrid laser beam welding-classification, characteristics, and applications. *J Laser Appl* 2006;18:169–80.

[19] Gao Z, Jiang P, Shao X, Cao L, Mi G, Wang Y. Numerical analysis of hybrid plasma in fiber laser-arc welding. *J Phys D Appl Phys* 2018;52:25206.

[20] Cho YT, Cho WI, Na S-J. Numerical analysis of hybrid plasma generated by Nd: YAG laser and gas tungsten arc. *Opt Laser Technol* 2011;43:711–20.

[21] Greses J, Hilton PA, Barlow CY, Steen WM. Plume attenuation under high power Nd: yttritium–aluminum–garnet laser welding. *J Laser Appl* 2004;16:9–15.

[22] Zou J, Yang W, Wu S, He Y, Xiao R. Effect of plume on weld penetration during high-power fiber laser welding. *J Laser Appl* 2016;28.

[23] Gray DE. American institute of physics handbook. 1972.

[24] Yamamoto K, Tanaka M, Tashiro S, Nakata K, Yamazaki K, Yamamoto E, et al. Numerical simulation of metal vapor behavior in arc plasma. *Surf Coatings Technol* 2008;202:5302–5.

[25] Murphy AB. The effects of metal vapour in arc welding. *J Phys D Appl Phys* 2010;43:434001.

[26] Murphy AB. A comparison of treatments of diffusion in thermal plasmas. J Phys D Appl Phys 1996;29:1922.

[27] Zhou J, Tsai HL, Lehnhoff TF. Investigation of transport phenomena and defect formation in pulsed laser keyhole welding of zinc-coated steels. *J Phys D Appl Phys* 2006;39:5338.

[28] Brent AD, Voller VR, Reid KTJ. Enthalpy-porosity technique for modeling convection-diffusion phase change: application to the melting of a pure metal. *Numer Heat Transf Part A Appl* 1988;13:297–318.

[29] Osher S, Fedkiw R. Level set methods and dynamic implicit surfaces. vol. 153. *Springer Science & Business Media*; 2006.

[30] Mu Z, Chen X, Zheng Z, Huang A, Pang S. Laser cooling arc plasma effect in laser-arc hybrid welding of 316L stainless steel. *Int J Heat Mass Transf* 2019;132:861–70.

[31] Kozakov R, Gött G, Schöpp H, et al. Spatial structure of the arc in a pulsed GMAW

process[J]. Journal of Physics D: Applied Physics, 2013, 46(22): 224001.

[32] Hao X, Liu L. Effect of laser pulse on arc plasma and magnesium target in low-power laser/arc hybrid welding. *IEEE Trans Plasma Sci* 2009;37:2197–201.

[33] Kawahito Y, Kinoshita K, Matsumoto N, Katayama S. Visualization of refraction and attenuation of near-infrared laser beam due to laser-induced plume. *J Laser Appl* 2009;21:96–101.

[34] Pang S, Chen X, Zhou J, Shao X, Wang C. 3D transient multiphase model for keyhole, vapor plume, and weld pool dynamics in laser welding including the ambient pressure effect. *Opt Lasers Eng* 2015;74:47–58.

[35] Pang S, Shao X, Li W, Chen X, Gong S. Dynamic characteristics and mechanisms of compressible metallic vapor plume behaviors in transient keyhole during deep penetration fiber laser welding. *Appl Phys A* 2016;122:702.